Robotica (2016) volume 34, pp. 1416–1435. © Cambridge University Press 2015
doi:10.1017/S0263574715000429

Calibration using adaptive model complexity for parallel and fiber-driven mechanisms

Tomáš Skopec, Zbyněk Šika* and Michael Valášek

CTU in Prague, Faculty of Mechanical Engineering, Department of Mechanics, Biomechanics and Mechatronics, Technická 4, Praha 6, 166 07, Czech Republic

(Accepted May 14, 2015. First published online: July 10, 2015)

SUMMARY

The paper deals with the development and application of a new adaptive calibration method that extends the geometrical calibration of mechanisms from calibration of only dimensions and kinematical joint positions into the calibration of kinematic joint shape imperfections. Originally unknown nonlinear properties of the kinematical pairs are adaptively included into the kinematical models that are used during the calibration calculation. The method uses description by local linear models and validity functions in order to identify and describe nonlinear properties of the kinematical pairs. During each calibration step, various models with growing complexity are considered before the best model variant is selected to improve calibration results. The method is mainly devoted to the structures with many loops like parallel and fiber-driven parallel mechanisms. The method is applied to parallel mechanism Sliding Star and parallel fiber-driven mechanism Quadrosphere.

KEYWORDS: Adaptive calibration method; Neuro-fuzzy calibration method; Nonlinear properties of kinematical pairs; Adaptive kinematical model; Parallel mechanisms; Fiber driven mechanisms.

1. Introduction

During the last few decades, there has been a large increase in the requirements for accuracy and productivity of all types of machines, especially for robots and machine-tools. A lot of new concepts and proposals of new machines have been developed. These new concepts, especially structures with parallel kinematics, might meet current tough requirements. The newly investigated extremely light variants of parallel structures are the fiber-actuated machines.[1–3] The traditional parallel as well as the fiber-driven parallel machines are characterized by many closed loops geometrically described by large set of parameters like dimensions and sensor offsets. The accurate determination of the exact values of these parameters is necessary for the accurate operation of machines.[4] Despite very precise manufacturing, it is not possible to use the design (blueprint) dimensions as parameters in the system control software. Usage of these dimensions would lead to inaccurate positioning of the machine end-effector that is connected to a working tool. Moreover, the actual (after assembly) values of these parameters cannot be directly measured, thus some indirect determination through the global measurement of the machine positioning is necessary. Some variant of the calibration method must be used to obtain the real dimensions of the machines and to improve their precision and accuracy.[5] The estimation method of the Stewart platform accuracy in different positions based on the positioning errors of actuators for their different extensions is developed in ref. [6].

Traditional calibration approaches use sets of mechanism measurements at various precisely determined positions. For each measurement, position values from all used drive sensors and possibly some other kinematical pairs as well, are obtained.

Calibration is an integrated procedure of modeling, measuring and then numerically identifying actual physical characteristics of a mechanism. Each calibration method consists of the following steps:[7]

* Corresponding author. E-mail: Zbynek.Sika@fs.cvut.cz

https://doi.org/10.1017/S0263574715000429 Published online by Cambridge University Press

1. Preparation of a calibration model.
2. Accurate measurement in various mechanism positions.
3. Reliable parameter and error identification using measurement data.
4. Compensation of identified errors and discrepancies.
5. Usage of the obtained parameter in control software, possible accuracy improvement.

Calibration methods might be divided into separate groups by the complexity of the calibration models used and by the level of knowledge of the calibrated mechanism.[8]

1.1. Level 1 calibration methods

A Level 1 calibration has been defined as "joint level" calibration. The purpose is to correctly relate a signal from a kinematical joint displacement transducer θ_r to an actual kinematical joint displacement θ_a. Many robots and mechanisms contain this calibration algorithm as a part of the start-up sequence and the process is referred as the initialization procedure.

1.2. Level 2 calibration methods

These calibration methods can be in general described as kinematical calibration of the mechanisms. Selected (or all) geometrical dimensions of the mechanism are computed during the calibration process that uses a kinematical model for a base for calibration computations. Used kinematical pairs are considered as lower kinematical pairs with unknown positions within the space of the machine. The actual positions of these kinematical pairs and other kinematical dimension are determined as calibration results. Majority of current calibration approaches falls into this category.

1.3. Level 3 calibration methods

As described in ref. [9], these calibration methods take into account both geometrical and non-geometrical sources of errors. The second group may consider additional model properties e.g. toughness of machine elements, friction, effects of temperature, dynamical parameters, etc. Usually only the toughness of selected elements is considered. Renders *et al.*[10] has considered the impact of other non-geometrical parameters, the most important is flexibility in the joints and in certain links that is responsible for 8–10% of the position and orientation error of the end effector. Angeles in ref. [11] analyzes the intrinsic properties of the Cartesian stiffness matrix in multibody systems. Calibration of the complex triple-level spatial positioner of radio waves receiver is the topic of paper.[12] One part of the story is the kinetostatic calibration of the large cable-driven parallel manipulator, which is necessary for the real-time cable tension optimization procedure used during the receiver motion planning. This approach represents an interesting example of level 3 calibration.

The calibration methods might be further divided into two groups according to the usage of an external measuring device to open and closed loop methods.

Open loop methods use various kinds of external measuring devices to obtain the both position and orientation of the end effector of the mechanism. For several mechanism positions, position of the end effector and data from the motion sensors are measured. Open loop calibration algorithms then use the measurement data and minimalize the differences between the positions measured by the external artifact and end effector positions that are computed from the sensor measurements.

Closed loop methods remove the usage of the external measuring devices and use the measurement data from the mechanism's inner sensors instead. This approach is usually called self-calibration or "online calibration" as no external tools are used.[4,13] In such cases, more sensors than the mechanism's degrees of freedom (DOF) are used. Self-calibration methods are suitable for calibration of the redundant parallel kinematic machines (PKM) because they might use existing sensors integrated within the mechanism's drives. The self-calibration with optimization of calibration positions of the fiber (cable) driven parallel robot with six DOF and eight drives is presented in ref. [14].

All current calibration methods consider the profiles of the kinematical joints as ideal and compute their absolute position within the mechanisms space. On the contrary, the presented new calibration method takes into account the possible nonlinear properties of the joints and adaptively constructs the neuro-fuzzy models that identify and describe these properties. The new method substantially extends and generalizes the possibilities of the adaptive polynomial calibration method presented by authors in ref. [15]. It uses several ideas from the LOLIMOT (Local Linear Model Tree)[16,17] algorithm during its calibration process; similar space division is used although the model construction strategy is

https://doi.org/10.1017/S0263574715000429 Published online by Cambridge University Press

completely different. The paper is divided into three main parts. After the Introduction section, the first part (Section 2) includes the basic formulation of the applied mathematical models and computations. The second part (Section 3) covers the theory and algorithm of the new calibration method and the last section (Section 4) demonstrates their usage on the two redundantly actuated parallel mechanisms. Both of them have four drives and three DOF. They are namely, the planar parallel mechanism Sliding Star[18,19] and the spherical parallel fiber-driven mechanism Quadrosphere.[20–22] The paper is closed by a brief conclusion.

2. Basis of used Modeling and Computation Methods

This section gives a brief overview of basic modeling and computations that are synergistically used by the new calibration method that is described in the next section.

2.1. Neuro fuzzy models

In order to model and subsequently calibrate the nonlinear properties of the calibrated mechanism, identification must take place. By identification of the system, we can construct an approximate model based on observation and basic knowledge of the system. The new calibration method described in Section 3.2 adaptively constructs neuro-fuzzy models in order to identify possible nonlinear properties of the kinematical joints.

Neuro-fuzzy networks combine advantages of both neuronal networks and fuzzy systems. In neuro-fuzzy networks, each neuron represents a *L*ocal *L*inear *M*odel (*LLM*) and it has associated a validity function that determines the region of validity of the LLM.[16] The output functions of the LLMs are

$$\hat{y}_i = w_{i0} + w_{i1}u_1 + w_{i2}u_2 + ... + w_{ip}u_p, \tag{1}$$

where w_{ij} are the LLM parameters of the neuron i and u_i are the coordinates of the input vector $\underline{u}$.

The ouptup of the whole system that consists of M local linear models is obtained as follows:

$$\hat{y} = \sum_{i=1}^{M} \underbrace{(w_{i0} + w_{i1}u_1 + w_{i2}u_2 + ... + w_{ip}u_p)}_{\hat{y}_i} \Phi_i(\underline{u}), \tag{2}$$

where $\underline{u}$ is a vector of system inputs ($\underline{u} = [u_1, u_2 \dots u_p]^T$) and $\Phi_i(\cdot)$ is a normalized validity function of the ith LLM. An important feature of the normalizated validity functions is that they form a partition of unity as

$$\sum_{i=1}^{M} \Phi_i\left(\underline{u}\right) = 1. \tag{3}$$

Normalized Gaussians are often chosen as the validity functions.[17] In case they are orthogonal, the validity functions are

$$\Phi_i\left(\underline{u}\right) = \frac{\mu_i(\underline{u})}{\sum_{j=1}^{M} \mu_j(\underline{u})}, \tag{4}$$

where

$$\mu_i\left(\underline{u}\right) = \exp\left(-\frac{1}{2}\left(\frac{(u_1 - c_{i1})^2}{\sigma_{i1}^2} + \frac{(u_2 - c_{i2})^2}{\sigma_{i2}^2} + \ldots + \frac{\left(u_p - c_{ip}\right)^2}{\sigma_{ip}^2}\right)\right). \tag{5}$$

Validity functions μ_i in Eq. (5) depend on the center coordinates c_{ij} and on the standard deviations σ_{ij}.

https://doi.org/10.1017/S0263574715000429 Published online by Cambridge University Press

2.2. Basic calibration algorithm

The closed kinematical loops equations mentioned above (or at least the virtual ones through the end-effector position on the calibration artifact) are used by level 2 calibration methods as follows. The kinematical loops are described by the kinematical constraint in the given position

$$\boldsymbol{f}\,(\boldsymbol{d}, \boldsymbol{s}, \boldsymbol{v}) = 0, \tag{6}$$

where $\boldsymbol{d}$ are actual dimensions of the mechanism ($\boldsymbol{d} = [d_1, d_2, \ldots, d_m]$, where m equals to the number of mechanism's dimensions), $\boldsymbol{s}$ are the measured joint coordinates and $\boldsymbol{v}$ are the output coordinates, i.e. the position of the end-effector.[23] The basic calibration algorithm uses Newton's method modified for over-constrained systems of nonlinear algebraic Eq. (24) that uses the constraint Eq. (6) for the measured data.

When $j = 1, \ldots n$ positions of the mechanism are considered, the constraint Eq. (6) are coupled into a system of constraint equations for the calibration algorithm

$$\boldsymbol{F}\,(\boldsymbol{d}, \boldsymbol{S}, \boldsymbol{V}) = 0, \tag{7}$$

where for the position j the constraint $\boldsymbol{f}_j = \boldsymbol{f}(\boldsymbol{d}, \boldsymbol{s}_j, \boldsymbol{v}_j) = 0$ and where $\boldsymbol{F} = [\boldsymbol{f}_1, \boldsymbol{f}_2, \ldots, \boldsymbol{f}_n]^T$, $\boldsymbol{S} = [\boldsymbol{s}_1, \boldsymbol{s}_2, \ldots, \boldsymbol{s}_n]^T$ and $\boldsymbol{V} = [\boldsymbol{v}_1, \boldsymbol{v}_2, \ldots, \boldsymbol{v}_n]^T$.

As mentioned in the previous section, for the non-redundant calibration approach the output coordinates $\boldsymbol{V}$ are measured by external devices. On the other hand, the (redundant) self-calibration approach does not necessarily require the output coordinates $\boldsymbol{V}$ to be used; position data from the sensors are sufficient. The Eq. (7) covers both the variants.

The calibration is based on the fact that the dimensions $\boldsymbol{d}$ are constant for all the positions. Unfortunately, the actual manufactured dimensions $\boldsymbol{d}$ are unknown as they differ from their design values $\bar{\boldsymbol{d}}$. Thus, the only unknown variables used in the Eq. (7) are the actual manufactured dimensions $\boldsymbol{d}$. This method is derived from the Taylor series of (7)

$$\boldsymbol{F}\left(\bar{\boldsymbol{d}}, \boldsymbol{S}, \boldsymbol{V}\right) + \boldsymbol{J}_d \delta \boldsymbol{d} + \ldots = 0 \tag{8}$$

with the Jacobi matrix $\boldsymbol{J}_d$ that consists of partial derivatives of the kinematical constraints (7) with respect to the calibrated dimensions $\boldsymbol{d}$. Hence after omitting the higher order members

$$\boldsymbol{J}_d \delta \boldsymbol{d} = -\boldsymbol{F}\left(\bar{\boldsymbol{d}}, \boldsymbol{S}, \boldsymbol{V}\right) = \delta \boldsymbol{r}. \tag{9}$$

The ith iteration step of Newton's method is

$$\delta \boldsymbol{d_i} = \left(\boldsymbol{J}_{d_i}^T \boldsymbol{J}_{d_i}\right)^{-1} \boldsymbol{J}_{d_i}^T \delta \boldsymbol{r}_i, \tag{10}$$

where $\boldsymbol{J}_{d_i}$ is the Jacobi matrix and $\delta \boldsymbol{r}_i = -\boldsymbol{F}(\boldsymbol{d}, \boldsymbol{S}, \boldsymbol{V})$ is a vector of deviations computed from the measured quantities and the calibrated quantities $\boldsymbol{d}_i$ obtained from the previous calibration step. New values of the dimensions are then computed as

$$\boldsymbol{d}_{i+1} = \boldsymbol{d}_i + \delta \boldsymbol{d}_i. \tag{11}$$

The iteration process continues while the deviations are decreasing and/or until a termination condition is satisfied.

As the described neuro-fuzzy calibration generates many calibration variants, a simple method that may be used for the classification of different calibration variants is required. The method uses calibrability as was proposed in ref. [19]. Calibrability C is obtained from the Jacobi matrix for the calibration step i and may be computed as follows:

$$C = cond\left(\boldsymbol{J}_{d_i}^T \boldsymbol{J}_{d_i}\right). \tag{12}$$

https://doi.org/10.1017/S0263574715000429 Published online by Cambridge University Press

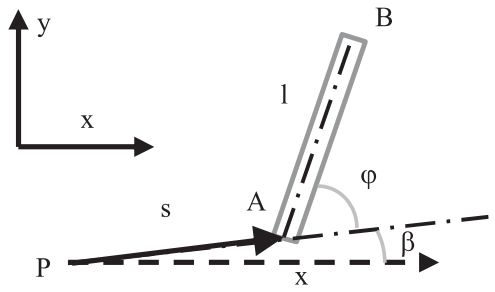


Fig. 1. Simple mechanism scheme.

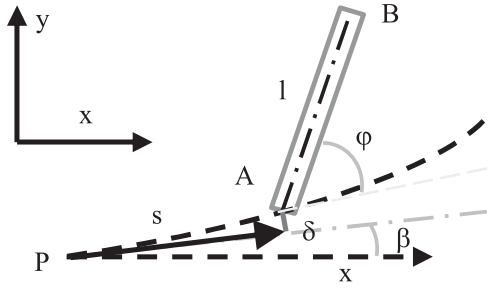


Fig. 2. Nonlinear kinematical joint.

Calibrability is a dimensionless number that gives us a better understanding of the calibrated system; it describes sensitivity of calibration dimension accuracy and an end-effector positioning accuracy with respect to the accuracy of the sensor measurements.

3. Synthesis of Adaptive Calibration Methods

This section describes several new adaptive calibration methods that use various approaches how to enhance the model used. At first, a simple adaptive method that uses polynomial models is described, then the models are described with neuro-fuzzy networks. An extension for redundant mechanism follows and a third-level variant of the calibration is also briefly explained.

3.1. Adaptive calibration with polynomial models

Adaptive polynomial calibration method is presented in this section as described by authors in ref. [15]. The main idea is to replace the ideal models of the kinematical joints with nonlinear models that adaptively adjust their complexity in order to improve overall calibration results.

In order to explain the application of the nonlinear models, application on a simple mechanism follows. The simple planar mechanism consists of the link l that carries working point B. The link is carried by the actuated prismatic pair guide (point A) that has its origin in point P (see Fig. 1).

The calibration method replaces the linear representation of the kinematical pair with the nonlinear model that may be considered as another element of the calibrated system (see Fig. 2).

The newly added member δ that represents the nonlinear properties of the associated kinematical pair is obtained from the used nonlinear model as

$$\delta = \delta\left(i_c, s\right), \tag{13}$$

where i_c is the index of calibration complexity and s is the position of the prismatic pair guide.

These nonlinear models might be represented by polynomial functions as described in ref. [15]

$$\delta = \delta\left(i_c, s\right) = \sum_{i_c} a_i s^{i+1}, \tag{14}$$

https://doi.org/10.1017/S0263574715000429 Published online by Cambridge University Press

where a_i are new parameters, that were adaptively introduced by the nonlinear models. They are *de facto* new calibration parameters as their values are computed during the calibration process.

The i_c member determines the level of nonlinear model complexity as described below. In the case of polynomial models, it determines the degree of polynomial member δ.

Equations for the coordinates of the point B are then

$$\begin{aligned} \boldsymbol{x}_B &= \boldsymbol{x}_P + \boldsymbol{s}\cos\boldsymbol{\beta} - \delta\left(i_c, \boldsymbol{s}\right)\sin\boldsymbol{\beta} + \boldsymbol{l}\cos\left(\phi + \boldsymbol{\beta}\right) \\ \boldsymbol{y}_B &= \boldsymbol{y}_P + \boldsymbol{s}\sin\boldsymbol{\beta} + \delta\left(i_c, \boldsymbol{s}\right)\cos\boldsymbol{\beta} + \boldsymbol{l}\sin\left(\phi + \boldsymbol{\beta}\right) \end{aligned}, \tag{15}$$

where the member δ adaptively increases its complexity during the calculation process.

Kinematical constraint Eq. (6) that is used during calibration is then

$$\begin{aligned} &\left(\boldsymbol{x}_{B_m} - \left(\boldsymbol{x}_P + \boldsymbol{s}\cos\boldsymbol{\beta} - \delta\left(i_c, \boldsymbol{s}\right)\sin\boldsymbol{\beta} + \boldsymbol{l}\cos\left(\boldsymbol{\phi} + \boldsymbol{\beta}\right)\right)\right)^2 \\ &\quad + \left(\boldsymbol{y}_{B_m} - \left(\boldsymbol{y}_P + \boldsymbol{s}\sin\boldsymbol{\beta} + \delta\left(i_c, \boldsymbol{s}\right)\cos\boldsymbol{\beta} + \boldsymbol{l}\sin\left(\boldsymbol{\phi} + \boldsymbol{\beta}\right)\right)\right)^2 = 0. \end{aligned} \tag{16}$$

The Jacobi matrix $\boldsymbol{J_d}$ that is used by Newton's method Eq. (10) is computed as partial derivatives of Eq. (16) for complete set of calibration positions.

As the calibration complexity index i_C increases, constraint equations' complexity changes according to i_C. The Eq. (14) shows, that $i_C + 1$ is the order of used polynomial function. Moreover, the number of the calibration parameters $\boldsymbol{d}$ is growing, because new parameters are introduced by the increase of the complexity of calibration model (more parameters a_i in eq. (14)). The same applies to the size of the Jacobi matrix $\boldsymbol{J_d}$ and the size of the differences vectors $\delta\boldsymbol{r}$ and $\delta\mathbf{d}$.

The adaptive behavior consists of controlled increases of the model complexity. The algorithm starts with a simple kinematical model and iteratively tries to increase its complexity (i.e. increase the complexity index i_c) in order to obtain better calibration results. An additional outer loop is added to the calibration algorithm that adaptively decides whether it is beneficial to increase complexity of the model.

Therefore, the adaptive calibration with polynomial models consists of two loops. The outer loop increases the complexity of the calibration model and the inner loop computes the dimensions of the model and the value of a ranking function. The outer loop continues until worse calibration results are obtained.

Progressive increasing of the kinematical model complexity is realized by increasing of the degree of the used polynomial. At some point, this might lead to a decrease of the calibrability, constrain equation discrepancies might increase and the obtained calibration results might be less accurate.

Several ranking functions may be used for a comparison of different calibration variants (for different values of the calibration index i_c) – e.g. a sum of all constraint equations discrepancies e (17), conditionality of the Jacobi matrix $\boldsymbol{J_d}$ or calibrability C (see Eq. 12).

$$e = \sqrt{\frac{\sum_n f\left(\boldsymbol{q}, \boldsymbol{z}, \boldsymbol{d}\right)^2}{n}}. \tag{17}$$

These ranking functions are used by a termination condition that is evaluated for each calibration variant. Therefore, it is able to determine whether the current calibration variant is more accurate than the previous one and to terminate the calibration algorithm when it is not beneficial to increase the complexity of the calibration model.

3.2. Adaptive calibration with neuro-fuzzy models

This section describes a new calibration method that uses neuro-fuzzy networks with a space division strategy that was introduced by the LOLIMOT algorithm. The main idea is the same as described by the polynomial calibration above – to replace unknown nonlinear behavior of the calibrated mechanism by kinematical models that adaptively increase their complexity.

When compared to the polynomial approach, the neuro-fuzzy networks are more capable in describing local nonlinear properties of the kinematical joints and their mathematical model remains simple even for complex nonlinear behaviors of the kinematical joints.

https://doi.org/10.1017/S0263574715000429 Published online by Cambridge University Press

Similarly to the LOLIMOT algorithm, this method divides input variables space and constructs local linear models that identify and approximate the nonlinear properties of the calibrated mechanism.

New logic is added to the calibration algorithm that gradually divides all input dimensions of all used adaptive models. For each variant, a new collection of the calibration dimensions $\boldsymbol{d}$ and a new calibration model are generated. For this calibration variant, calibrated dimensions are obtained and a value of selected ranking function is computed. Lastly, for the selected calibration complexity index i_c (i.e. number of input space divisions), the best possible variant is chosen from comparison of the ranking values and this variant is then used as a starting point for the next calibration step with an increased value of the calibration index i_c.

The logic of the adaptive calibration algorithm may be divided into following steps:

1. *Create an initial calibration model*: Generate validity functions for the initial input space partitioning.
2. *Generate a collection of available calibration variants*: Iterate through all available input space partitioning variants for the given calibration complexity i_c. As the structure of the calibrated model changes, it is required to execute following sub-steps.
   a Compute the membership functions μ, according to Eq. (5), for the current space partitioning.
   b Compute the normalized validity functions Φ_i for all current LLMs according to (4) with respect to (3).
   c Obtain values of the parameters w_{ij} by calibration of the current calibration model.
      i Add the new calibration parameters for the actual variant to the collection of the calibration parameters $\boldsymbol{d}$.
      ii Generate a new form of the constraint Eq. (16) and Jacobi matrix $\boldsymbol{J}_d$.
      iii Calibrate the actual variant.
   d Determine value of the ranking function for the given variant according to Eqs. (12) and (17).
3. *Select the best available variant*: Select the best input space partitioning variant with the lowest rank for the current value of the calibration complexity index i_c.
4. *Test for convergence*: Check whether it is reasonable to continue with the increasing of the calibration index i_c using the logic described above. If the selected best variant has lower values of the ranking function, increase the value to the index $i_c = i_c + 1$ and continue with the iterations – return to step 2.

For same of simplicity, the algorithm flow can be expressed with a simple flowchart (see Fig. 3).

There is an important difference how the parameters w_{ij} are computed when compared to the LOLIMOT algorithm. The calibration algorithm needs to calibrate the calibration model during execution of the inner calibration loop. On the other hand, the LOLIMOT algorithm simply uses the method of least squares.

The LOLIMOT algorithm (and other growing algorithms) uses ranking criteria that are available for each individual local linear model. This calibration method lacks this option therefore it obtains values of the ranking functions for all available calibration variants. The best input space partitioning variant is then selected and it is subsequently used as a starting point for the next possible iterations.

In other words, the calibration method systematically searches all available input space divisions and evaluates their values of the ranking functions from the calibration of the corresponding variant. Then the best variant is selected and used during the next search loop.

3.3. Adaptive neuro-fuzzy calibration of redundant parallel mechanisms

This section describes a modification of the neuro-fuzzy calibration method and extends it for application to redundant parallel mechanisms.

The application lies in replacement of r kinematical pairs by corresponding number of separated neuro-fuzzy models. Each model uses a position of the related kinematical pair as an input variable, therefore its input space is only one-dimensional and the partitioning is separated. Each model represents a SISO (Single-Input, Single-Output) system. Each model l has its own center coordinates $c_i^{(l)}$, LLM weight parameters $w_{ij}^{(l)}$ and validity functions $\Phi_i^{(l)}$, where $l = (1, \ldots, r)$.

https://doi.org/10.1017/S0263574715000429 Published online by Cambridge University Press

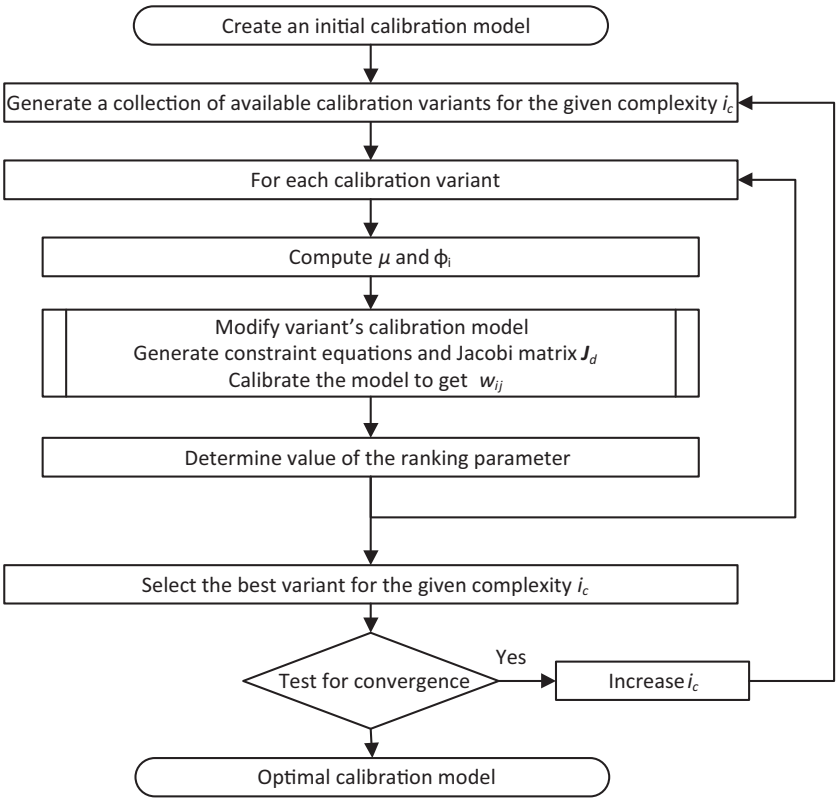


Fig. 3. Calibration algorithm flow chart.

The overall output y_l of a SISO model of one kinematical pair is then

$$\hat{y}_l = \sum_{i=1}^{M_l} \left(w_{i0}^{(l)} + w_{i1}^{(l)} u_1 \right) \Phi_i^{(l)}(u_1). \tag{18}$$

Redundant mechanisms are usually calibrated by closed loop calibration methods as mentioned in Section 1. If all the used loops use at least one neuro-fuzzy model described by Eq. (18), as there is no external measuring device that would "lock" the mechanism position, the absolute position in the space of the mechanism would become ambiguous. Therefore, it is necessary to "lock" at least one LLM of one model of a kinematical pair. This can be easily done by the removing of all parameters of the selected LLM from the collection of calibrated parameters $\boldsymbol{d}$, so that the parameters would not change during calibration. During the selection of the best available variant for the given value of the calibration complexity index i_c, two following approaches were considered.

Globally increased complexity of all models – Just one global complexity index i_c is used for all the models, therefore one LLM in each model is divided into two new LLMs. Therefore, all models contain exactly the same number of LLMs that is equal to the value of the calibration complexity index i_c.

Selectively increased complexity of individual models – All possible divisions of all models are also considered during each iteration step, but just one LLM of one model is then divided into two new LLMs. In contrast to the previous approach, it is possible that LLMs of one model are divided as long as it provides better calibration results. During the next steps, other LLMs of other models may be divided. A sum of all LLMs of all models is equal to the value of the index i_c.

3.4. Level 3 adaptive neuro-fuzzy calibration

If we modify the neuro-fuzzy networks used for nonlinear properties behavior so that they will consider e.g. position of the mechanism working platform or position of the other actuators as the input parameters, we should be able to describe and calibrate even some non-geometrical sources

https://doi.org/10.1017/S0263574715000429 Published online by Cambridge University Press

of the positioning errors. If we use the position of the mechanism working platform, the calibration method will be able to describe the influence of flexibility of mechanism members; we will obtain a level 3 calibration method (see Section 1). The dimensions slightly differ between the particular positions within the workspace because of the different static loading by the gravity forces and the mechanism flexibility. Consequently, the position of the working platform can be used for the parameterization of the static deformation change of the dimensions.

Each model (neuro-fuzzy network) will have p inputs and the input parameters vector u will be defined as $\boldsymbol{u} = (u_1, \ldots, u_p)$. Thus, in this case, all models will use the same input vector $\boldsymbol{u}$ and the whole system might be considered as a system with multiple inputs and multiple outputs. The system might be realized by a set of separated MISO models (*Multiple Input, Single Output*) or by a MIMO model (*Multiple Input, Multiple Output*).

When the set of separated MISO models is used, output equations of the individual networks $\hat{y}_l$ have the following form:

$$\hat{y}_l = \sum_{i=1}^{M_l} \left(w_{i0}^{(l)} + w_{i1}^{(l)} u_1 + w_{i2}^{(l)} u_2 + \ldots + w_{ip}^{(l)} u_p \right) \Phi_i^{(l)}(\boldsymbol{u}). \tag{19}$$

An alternative approach uses the MIMO model where each neuron realizes an LLM for each output $\hat{y}_l$. In that case, there is only one shared neuronal network structure, only one shared partitioning of the input space dimensions and, in the end, only one set of the validity functions $\Phi_i (i = 1, \ldots, M)$ is used.

In contrast to Eq. (19), the output $\hat{y}_l$ for selected network of l has following form:

$$\hat{y}_l = \sum_{i=1}^{M_l} \left(w_{i0}^{(l)} + w_{i1}^{(l)} u_1 + w_{i2}^{(l)} u_2 + \ldots + w_{ip}^{(l)} u_p \right) \Phi_{\mathrm{i}}(\boldsymbol{u}). \tag{20}$$

The greatest disadvantage of the first approach is a rapid increase of its computational complexity due to the much higher number of possible input space divisions and calibrated variants. As the values of $\boldsymbol{u}$ are common for all the network structures (they were obtained at once during a calibration measurement), it is very probable that all the nonlinearities of output functions share the same properties for the given space division. Therefore, the second approach was applied to all simulations and experiments. The level 3 variant of adaptive neuro-fuzzy calibration is useful for mechanisms, where the deformations are important for the final accuracy and/or the deformations can be measured by the additional sensors.

4. Applications of Adaptive Calibration Methods

This section describes applications of the newly developed calibration method. At first, an application on redundant parallel mechanism Sliding Star is described, covering several calibration approaches. The second part of this section describes an application on spatial fiber-driven mechanism Quadrosphere. These two examples illustrate the usage of the method for the components taken into account differently for different types of mechanisms. For Sliding Star mechanism, an adaptive model of translational joint is formulated for the planar kinematics, whereas in Quadrosphere the adaptive model is set up for the spatial motion. Similarly to the translational joints also the deviation of the ideal shape of revolute, spherical or other joints can be analogically described by the neuro-fuzzy models. Long translational joints have been chosen for the pilot applications of the method because of their often significant deviations from the ideal linear shapes. The level 3 variant of the method is currently under development for the calibration of the robotic arm (Fig. 4(a)) equipped with the additional sensors. Internal sensors in drives, sensors directly in joints and links deformation sensors are considered. Deformations of the long links of the arm will be detected by the four quadrant-detectors of the spots of the laser beams (Fig. 4(b)). The adaptive calibration will use the synchronous data from the laser-tracker measurement of the motion of endpoint **E** (with mounted trigonal reflector) and the data from all internal arm sensors. The aim is to tune appropriate complexity of the model

https://doi.org/10.1017/S0263574715000429 Published online by Cambridge University Press

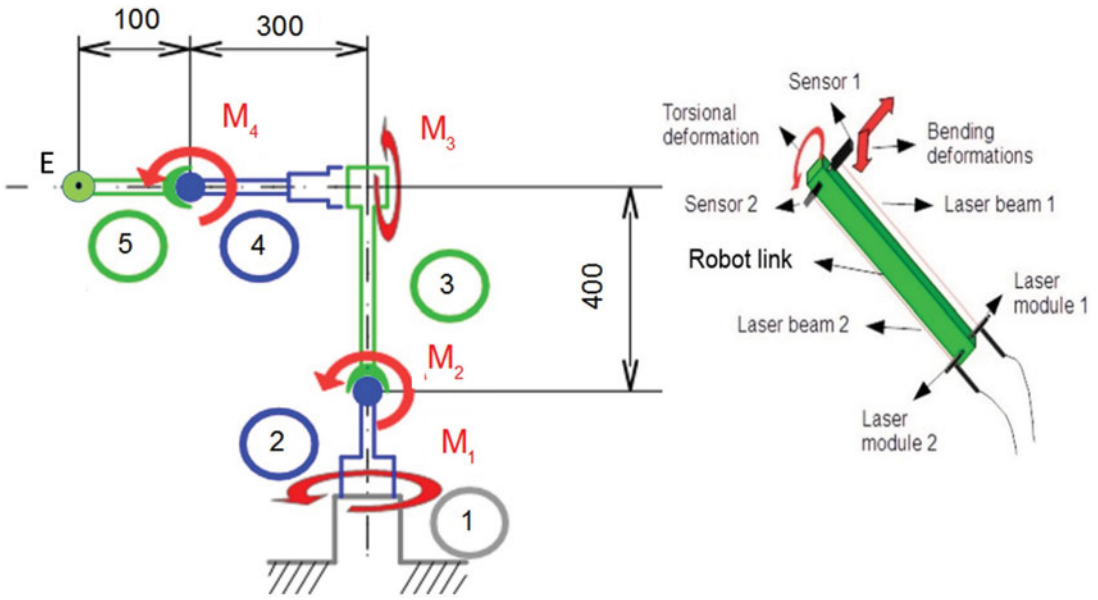


Fig. 4. Model of flexible robotic arm with additional deformation sensors. (a) Scheme of experimental arm. (b) Scheme of link deformation measurements.

for the evaluation of the endpoint motion based on the internal sensors outputs including the links deformation sensors outputs.

4.1. Adaptive calibration of redundantly actuated parallel mechanism Sliding Star

As stated above, the new calibration approaches were experimentally verified by calibration of mechanism Sliding Star.[18,19] It is a planar redundant parallel mechanism with four prismatic kinematical pairs s_i and eight revolute kinematical pairs φ_i and ψ_i (see Fig. 5). The prismatic pairs are realized by translation of four carts that are actuated by four drives, the working platform $B_1B_2B_3B_4$ has the number of DOF equal to 3; translation in the directions of both x-axis and y-axis, rotation around an axis perpendicular to the moving platform (Fig. 6). Because the number of actuated drives is higher than its DOF, the mechanism is redundant; in other words, the machine is using a redundant link. A functional prototype of Sliding Star mechanism for an experimental verification of the adaptive calibration algorithm was used (Fig. 5). Size of the square shaped moving platform is **0.4 m** $\times$ **0.4 m**, length of the links $|S_1B_1|$ and $|S_3B_3|$ is **0.6 m**, length of the links $|S_2B_2|$ and $|S_4B_4|$ is **0.85 m** respectively. Height of the mechanism h (distance between the prismatic pairs) is **1.02 m**. In order to perform calibration measurements, it is necessary to develop and implement a mechanism control system. A decentralized control approach was selected and it was implemented in the flexible rapid prototyping controller system dSpace in combination with the numerical computing system Matlab/Simulink. A grid containing approximately 300 positions of the working platform (end-effector) that cover the whole mechanism working space was used to measure values of the prismatic pair coordinates $s_1 - s_4$ and the revolute pair coordinates $\varphi_1 - \varphi_4$.

The measured coordinates were used for neuro-fuzzy calibration, with the second complexity increase approach applied. Four independent SISO models were added to the mechanism kinematical model, the members δ in Eq. (14) are then

$$\delta_l = \delta_l(s_l) = \sum_{i=1}^{M_l} \left(w_{i0}^{(l)} + w_{i1}^{(l)} s_l \right) \Phi_i^{(l)}(s_i), \tag{21}$$

where the member l stands for an index of the modeled prismatic kinematical pair; $l = (1, 2, 3, 4)$.

https://doi.org/10.1017/S0263574715000429 Published online by Cambridge University Press

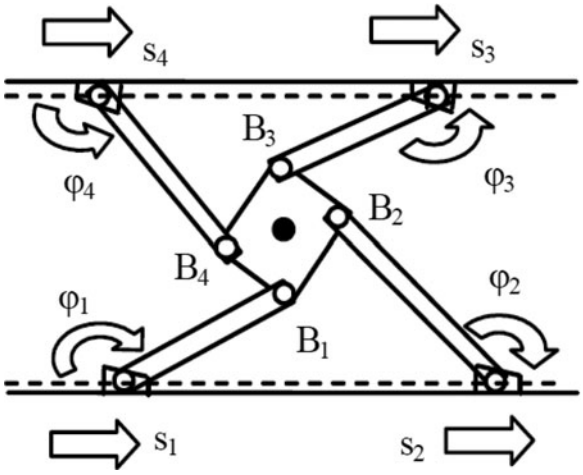


Fig. 5. Sliding Star – scheme.



Fig. 6. Sliding Star – adaptive calibration of prototype.

Equations that might be used to obtain coordinates of the points B_i are analogous to Eq. (15) and are used to define boundary conditions as

$$\begin{gathered}
\left(x_{B_1} - x_{B_2}\right)^2 + \left(y_{B_1} - y_{B_2}\right)^2 - \xi_{B_2}^2 = 0 \\
\left(x_{B_1} - x_{B_3}\right)^2 + \left(y_{B_1} - y_{B_3}\right)^2 - \xi_{B_3}^2 - \eta_{B_3}^2 = 0 \\
\left(x_{B_2} - x_{B_3}\right)^2 + \left(y_{B_2} - y_{B_3}\right)^2 - \left(\xi_{B_3} - \xi_{B_2}\right)^2 - \eta_{B_3}^2 = 0 \\
\left(x_{B_2} - x_{B_4}\right)^2 + \left(y_{B_2} - y_{B_4}\right)^2 - \left(\xi_{B_4} - \xi_{B_2}\right)^2 - \eta_{B_4}^2 = 0 \\
\left(x_{B_3} - x_{B_4}\right)^2 + \left(y_{B_3} - y_{B_4}\right)^2 - \left(\xi_{B_4} - \xi_{B_3}\right)^2 - \left(\eta_{B_4} - \eta_{B_3}\right)^2 = 0.
\end{gathered} \tag{22}$$

The boundary conditions are defined for the working platform coordinate system (ξ, η) and represent relations between its points B_i. During the calibration that follows the same algorithm as described in the Section 3.2, new symbolic equations for the Jacobi matrix $\boldsymbol{J}_d$ and new boundary conditions were generated for each calibration variant. The Fig. 7 contains the calibration results; it contains nonlinear geometrical deviations from the linear shape of the prismatic pair trajectories. Based on their shape, it is obvious that the neuro-fuzzy calibration algorithm is able to obtain more

https://doi.org/10.1017/S0263574715000429 Published online by Cambridge University Press

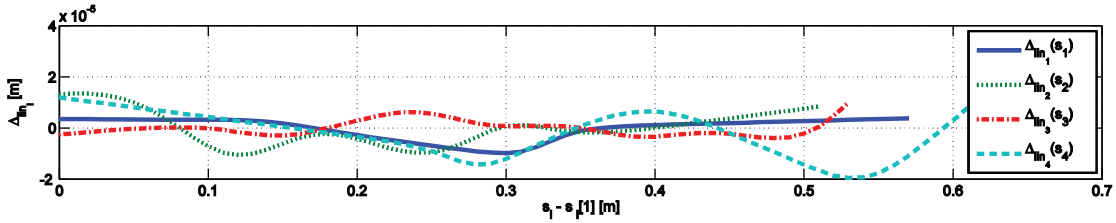


Fig. 7. Sliding Star – deviations from the linear shape of the prismatic pairs calibrated from measurements.

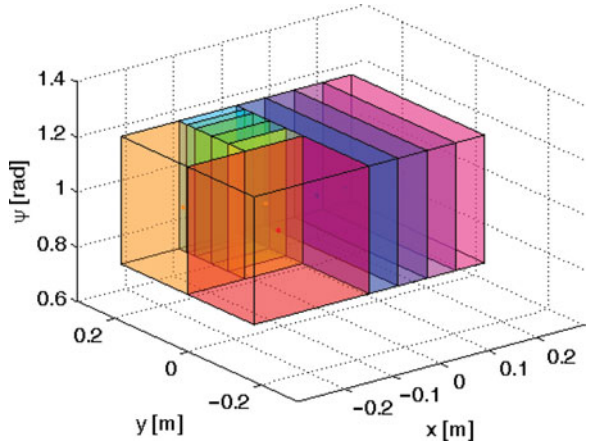


Fig. 8. Level 3 – input space partitioning.

detailed information about the calibrated mechanism and therefore acquire more accurate knowledge of the machine motion. Namely the results of the presented adaptive calibration of the Sliding Star have been used within the applied control algorithm for the motion control of this machine by a redundant number of drives.

In general, a further possible step of the calibration improvement is the usage of the third-level calibration, which enables to take into account some non-geometrical sources of the positioning errors as described within the Section 3.4. The most important agent of such non-geometric source of errors is the mechanism's flexibility. The geometrical parameters generally differ between the particular calibration (and afterwards working) positions within the workspace because of the different static loading by the gravity forces and the mechanism flexibility. Consequently, the position of the working platform represents the natural parameterization of the static deformation change of the geometrical parameters. There are also other factors as the temperature or backlashes in joints, but these effects are typically of less importance.

This approach was evaluated for Sliding Star calibration, the input space was partitioned during the adaptive calibration as displayed in Fig. 8; an additional terminal condition that limits the maximal count of all LLMs and input space divisions were added ($llmMax = 10$). This partitioning can indicate which part of the mechanism's working space shows the most nonlinear properties and when combined with the obtained results for the nonlinear adaptive model δ_2 displayed in Fig. 9 (plane x_N, y_N with a chosen value of the working platform rotation $\psi = 1$rad), the most nonlinear area of the working space due to mechanism's flexibility is for $-0.2 < x < 0m$ and $0 < y < 0.2m$. However, for the Sliding Star mechanism, the third-level calibration does not bring further improvement of the accuracy. Therefore, as mentioned above, the results of *geometrical adaptive calibration* described by Fig. 7 have been used for the machine control.

4.2. Adaptive calibration of redundantly actuated fiber-driven mechanism Quadrosphere

A spatial variant of the adaptive calibration approach has been applied to a mechanism called Quadrosphere. It is an innovative fiber-driven parallel mechanism that uses fibers instead of struts. Because fibers are lighter than the traditional materials, light and fast parallel mechanisms can be created. As fibers cannot transfer stress, tension must be applied all the time (so called anti-backlash

https://doi.org/10.1017/S0263574715000429 Published online by Cambridge University Press

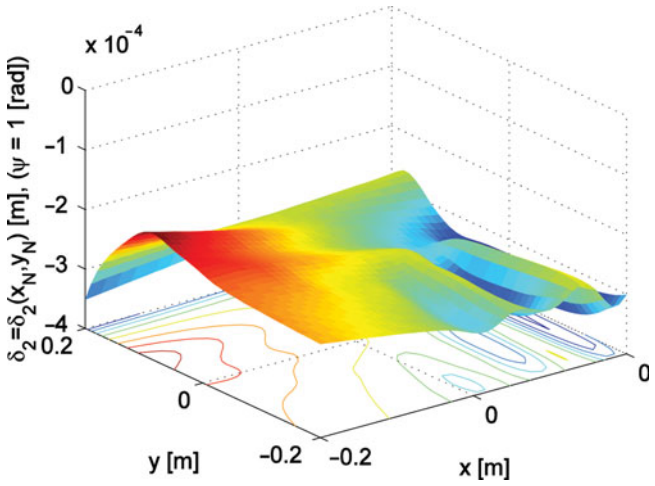


Fig. 9. Level 3 – results for δ_2.

control),[20] otherwise the mechanism would collapse. The fiber-driven mechanism Quadrosphere (Fig. 11) follows a concept of the rod or fiber-driven redundant parallel mechanism called Hexasphere (Fig. 10) that is described in refs. [2] and [21]. The working platform is connected to the frame by a central spherical joint. The mechanism has three DOF, therefore just three actuators would suffice to move the platform. However, they would enable motion in just a small extend of angles, because for wider angles singular positions occur. When the platform is supported by more rods or fibers, singular positions are removed and overall better kinematical properties are acquired.[22] Mechanism Quadrosphere uses the same concept as mechanism Hexasphere, but first the fibers are used instead of the rigid rods and secondly their number is reduced from 6 to 4. Moreover, the central spherical joint is equipped with three revolute sensors (Fig. 11). Namely, the RENISHAW RESM Signum angular encoder system is used, which consists of a ring (basic increment 20μm) and the interpolator. The drawback of initial Hexasphere model is the lack of sensors for the platform orientation (Fig. 12). The high importance of the platform position measurement has been detected both for the good calibrability and for its position control. Quadrosphere can be also considered as a fiber-driven alternative of mechanism from ref. [25]. When compared to Hexasphere, there is a slight decrease in stiffness and the anti-backlash working space, however the slight deterioration of the mechanical properties is compensated by reduction of the number of drives.[20] The Figs. 12 and 13 compare the kinematical schemes of both mechanisms. In order to calibrate spatial redundant parallel mechanism Quadrosphere, a spatial variant of the adaptive calibration algorithm has been developed.

The nominal dimensions of the Quadrosphere mechanism are as follows, the diameter of the circle of the frame points P_i is $d_P = \mathbf{1{,}199\ m}$, the diameter of the circle of points C_i on the working platform is $d_C = \mathbf{0{,}438\ m}$, the distance from the center of spherical joint to working platform circle plane PS $= \mathbf{0{,}180\ m}$. The working platform of the mechanism is connected to the frame by a central spherical joint that might be described by three Euler angles φ, θ, ψ. Its position is determined by position of sliders on four prismatic pairs s_i that are realized by translation of four carts actuated by four drives. Constraint conditions that are used during the calibration of the mechanisms describe relation between positions of points A_i and C_i and lengths of fibers l_i. The positions of points C_i might be represented by Euler angles φ, θ, ψ with the matrix notation as follows.

$$\boldsymbol{r}_{C_i}^{I} = \boldsymbol{T}_{\varphi_z}(\psi)\,\boldsymbol{T}_{\varphi_x}(\theta)\,\boldsymbol{T}_{\varphi_z}(\varphi)\,\boldsymbol{r}_{C_i}^{II}, \tag{23}$$

where vector $\boldsymbol{r}_{C_i}^{II}$ describes position of points C_i in the coordinate system (x_2, y_2, z_2) and $\boldsymbol{r}_{C_i}^{II} = [x_{C_i}^{II}, y_{C_i}^{II}, z_{C_i}^{II}, 1]^T$ as displayed in Fig. 13.

Calibrated position of points A_i is influenced by considered orientation of the prismatic pairs $\varphi_{x_{P_i}}, \varphi_{y_{P_i}}$ and then is described as

$$\boldsymbol{r}_{A_i}^{I} = \boldsymbol{T}_{\varphi_x}\left(\varphi_{x_{P_i}}\right)\boldsymbol{T}_{\varphi_y}\left(\varphi_{y_{P_i}}\right)\boldsymbol{r}_{A_i}, \tag{24}$$

https://doi.org/10.1017/S0263574715000429 Published online by Cambridge University Press

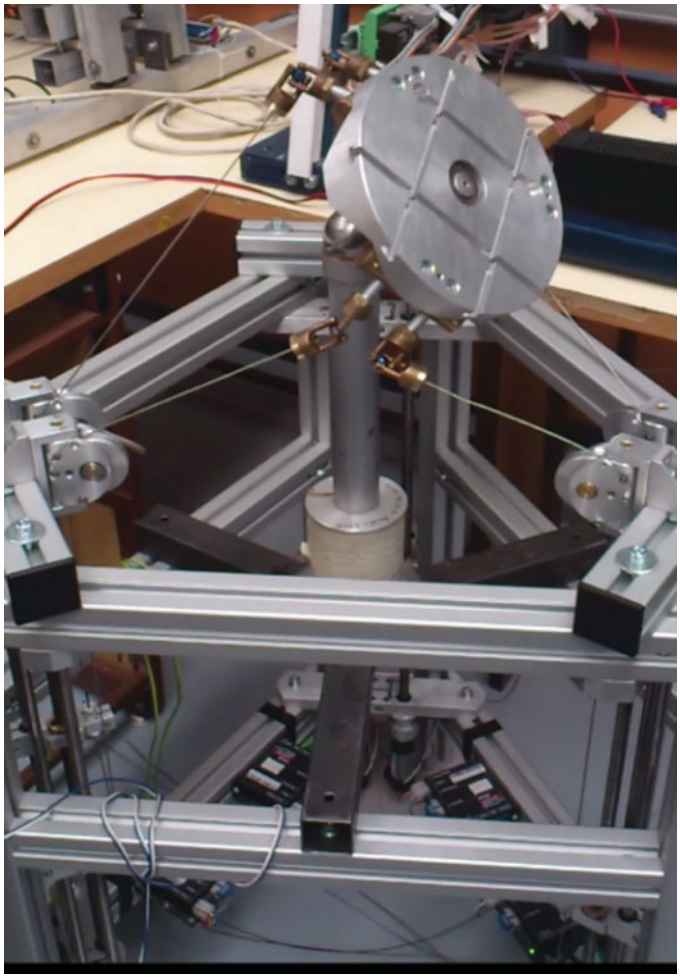


Fig. 10. Fiber-driven mechanism Hexasphere without spherical position sensors.

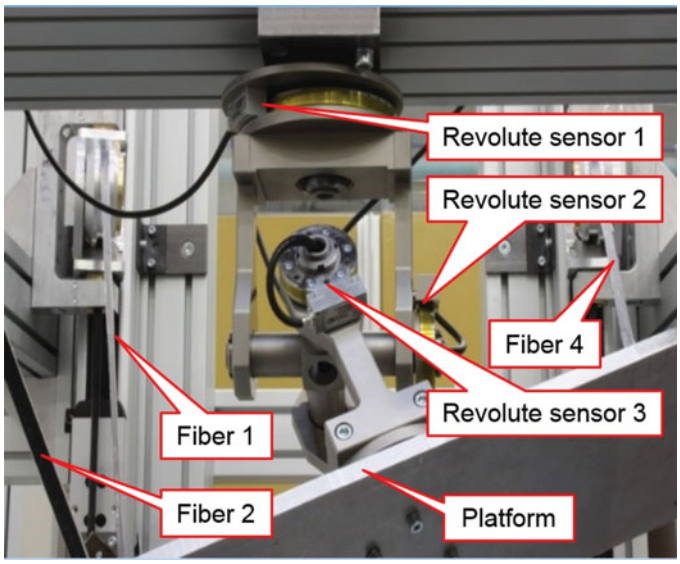


Fig. 11. Fiber-driven mechanism Quadrosphere with spherical position sensors.

https://doi.org/10.1017/S0263574715000429 Published online by Cambridge University Press

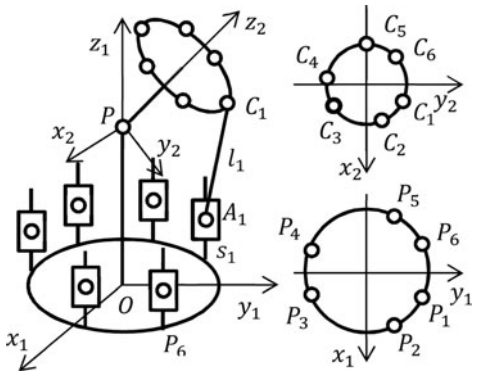


Fig. 12. Hexasphere – kinematical scheme.

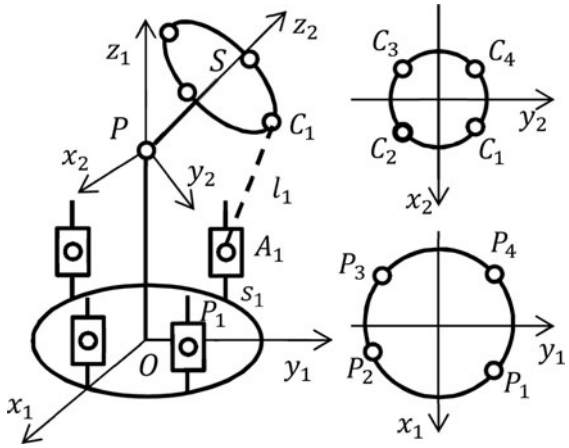


Fig. 13. Quadrosphere – kinematical scheme.

where $\boldsymbol{r}_{A_i}$ is the position of the points A_i in the coordinate system (x_1, y_1, z_1) and $\boldsymbol{r}_{A_i} = [x_{A_i}, y_{A_i}, z_{A_i}, 1]^T$.

The boundary conditions are then assembled for each fiber of the mechanism in the following form:

$$\left(x_{C_i}^I - x_{A_i}^I\right)^2 + \left(y_{C_i}^I - y_{A_i}^I\right)^2 + \left(z_{C_i}^I - z_{A_i}^I\right)^2 - l_i^2 = 0. \tag{25}$$

For a simulation of the mechanism calibration, a grid with more than 150 positions of the working point was used. During a simulation of a calibration measurement, a given set of the Euler angles φ, θ, ψ values was used as input to a numerical inverse kinematic problem. As a result, corresponding positions of the prismatic pairs s_i was obtained.

Based on the calibration measurement setup that operates with sets of values of s_i and φ, θ, ψ, the following mechanism dimensions were determined as calibration parameters:

- x_0, y_0, z_0 - Coordinates of the central spherical joint
- $x_{C_i}^{II}, y_{C_i}^{II}, z_{C_i}^{II}$ - Coordinates of points C_i on the working platform
- $x_{P_i}, y_{P_i}, z_{P_i}$ - Coordinates of frame points P_i
- l_i - Lengths of the connecting fibers between the frame and the working platform
- $\varphi_{x_{P_i}}, \varphi_{y_{P_i}}$ - Orientation of the prismatic kinematical pairs

When we apply the adaptive neuro-fuzzy calibration approach, the spatial prismatic kinematical pairs are modeled by four independent sets of perpendicular pairs of planar SISO models in planes xz and yz. Therefore, each SISO model describes possible nonlinear properties of the kinematical pair in either dimension x or dimension y. The final model of each spatial prismatic kinematical pair is then obtained by application of the superposition principle to both of its SISO models. As each of the kinematical pairs is replaced by a set of adaptive neuro-fuzzy models, some of the

https://doi.org/10.1017/S0263574715000429 Published online by Cambridge University Press

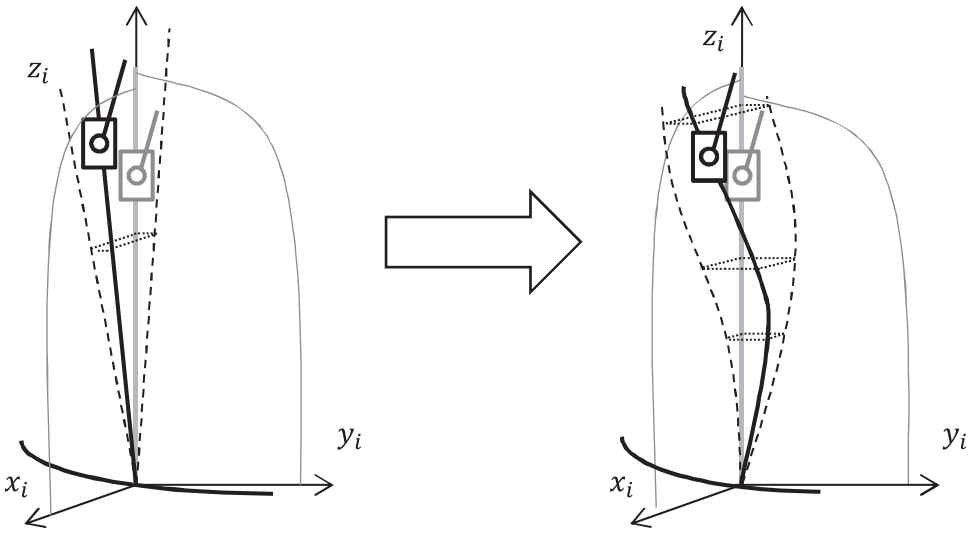


Fig. 14. Adaptive neuro-fuzzy identification of a Quadrosphere prismatic kinematical pair i.

calibration parameters become parameters of the neuro-fuzzy models that are also determined during the calibration process. Coordinates x_{A_i} and y_{A_i} of the points A_i are described by absolute LLM parameters w_{i0} and the orientation of the prismatic pairs is described by linear LLM parameters w_{i0}. It is not possible to calibrate all coordinates as some of them must be used to determine mechanism's absolute position and orientation in space. For Quadrosphere, following variables were selected to describe the position and therefore removed from the calibration process.

- $x_{C_1}, y_{C_1}, z_{C_1}$ - Absolute position of point C_1
- $\varphi_{x_{A_1}}, \varphi_{y_{A_1}}$ - Orientation of the first spatial prismatic pair
- x_{C_2} - Determines the final absolute position of the mechanism

Figure 14 contains a scheme of a calibration model for each of the Quadrosphere prismatic kinematical pairs and an idea of its development during the calibration process.

Each time, when the complexity of the calibration model i_c increases, new Local Linear Models are added to each pair of the planar SISO models that represent the spatial prismatic pairs. As mentioned in Section 3.2 step 2, all available space partitioning variants should be considered for the given calibration complexity i_c. As mentioned above, the complexity and therefore the number of calibrated parameters increases during the calibration. With each increase of calibration complexity i_c the following set of variables is generated for each leg of the mechanism.

- $w_{M0}^{(l,x)}$ - Absolute weight parameter of Mth LLM for x-dimension SISO model of leg l
- $w_{M1}^{(l,x)}$ - Linear weight parameter of Mth LLM for x-dimension SISO model of leg l
- $w_{M0}^{(l,y)}$ - Absolute weight parameter of Mth LLM for y-dimension SISO model of leg l
- $w_{M1}^{(l,y)}$ - Linear weight parameter of Mth LLM for y-dimension SISO model of leg l

For Quadrosphere, a set of 16 (4 parameters per leg) is added each time the complexity of calibration is increased. That also means that 16 new partial derivatives of 4 boundary conditions are computed as a part of the calibration system Jacobi matrix.

In order to reduce number these variants and to reduce computational complexity, we can assume that degree of nonlinearity of a spatial prismatic pair is similar for both planar SISO models that describe it. Therefore, the space partitioning is common for both models of the prismatic pair and number of calibration variants is significantly reduced. Simulation of the calibration measurement was performed (see Fig. 15) in order to tune the calibration algorithm. The convergence of the Quadrosphere adaptive neuro-fuzzy calibration is very fast as displayed in Fig. 16.

The developed calibration algorithm has been used for the evaluation of the accurate parameters of the Quadrosphere mechanism which are necessary for the control by redundant number of drives similarly as for the Sliding Star mechanism. The calibrated parameters are used within the Inverse

https://doi.org/10.1017/S0263574715000429 Published online by Cambridge University Press

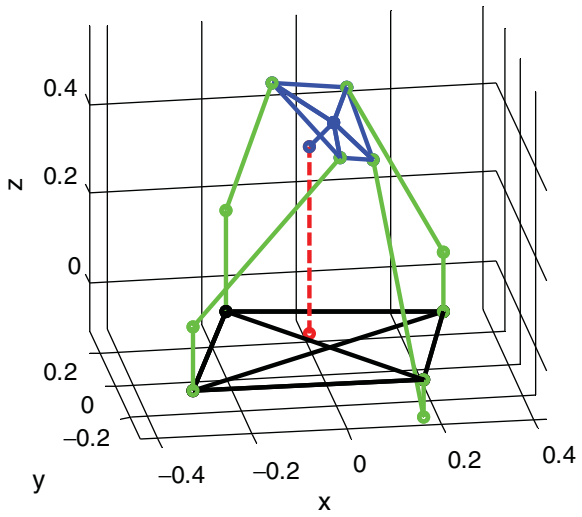


Fig. 15. Testing of algorithm for inexactly mounted Quadrosphere mechanism.

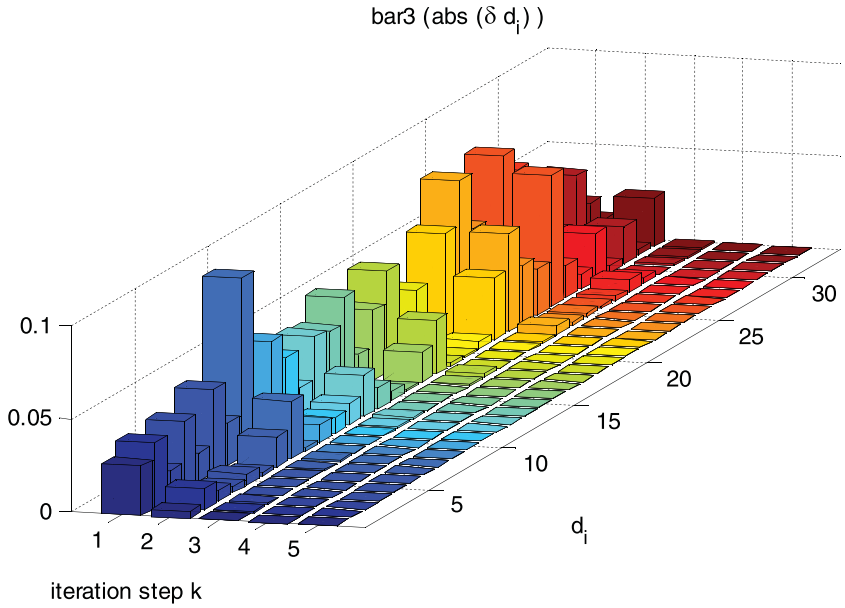


Fig. 16. Convergence of neuro-fuzzy Quadrosphere calibration.

kinematic blocks (Fig. 17) in the control algorithm. The controller obtains the actual spherical position of the platform based on the signals from the joint incremental sensors. Three of four drives are controlled directly from the inverse kinematics, the fourth drive is controlled in order to stabilize the fiber tension measured by the force sensor. The position control including the inverse kinematic is realized in the higher level global controller (dSpace), whereas the velocity and current loops of drives are realized by the local controllers (LXM1, LXM2, LXM3, LXM4).

5. Conclusion

The new calibration method has been investigated in the presented paper. This new approach for the first time in the literature enables to carry out the mutual calibration with adaptive complexity of both dimension of mechanism and the real shape of kinematic joints. The method enables to significantly reduce the uncertainty level of calibration and increase the level of deterministic description of mechanisms. The model is dynamically extended with local linear model tree nodes that are used to identify and describe nonlinear properties of the kinematical pairs of the calibrated mechanism. The

https://doi.org/10.1017/S0263574715000429 Published online by Cambridge University Press

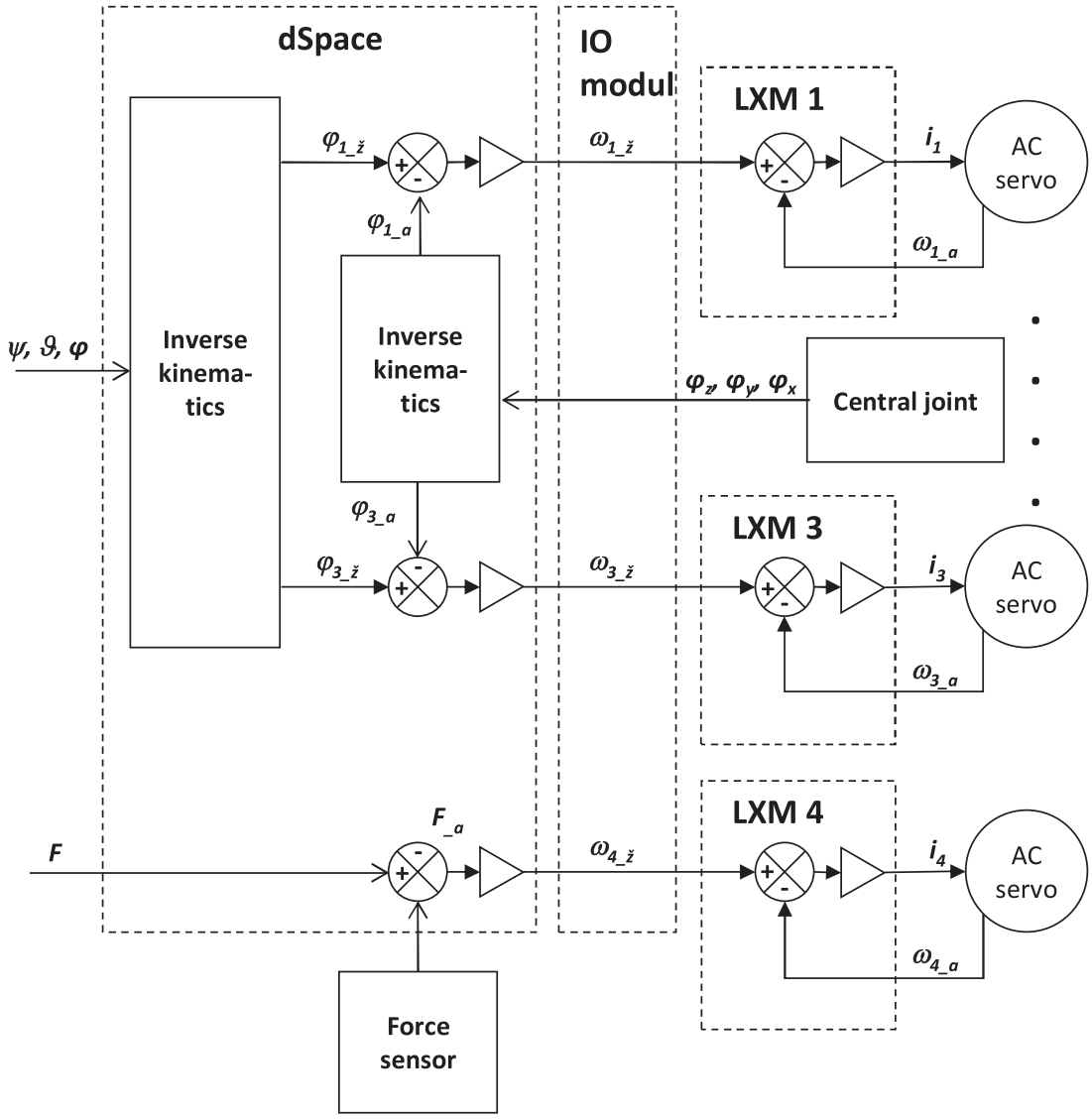


Fig. 17. Structure of Quadrosphere mechanism control.

main idea is to gradually extend the calibration model and to find optimal ratio between complexity of the model and the calibration results. A detailed description of the calibration algorithm and individual steps of the calibration process has been presented. The method has been extended for calibration of redundant parallel mechanisms and a variant of level 3 calibration of non-geometrical parameters has been discussed. The level 3 variant of adaptive neuro-fuzzy calibration is useful for mechanisms, where the deformations are important for the final accuracy and/or the deformations can be measured by the additional sensors. The application of the level 3 variant of the method is currently under development for the calibration of the experimental flexible robotic arm. The usage of the adaptive calibration method has been demonstrated by experimental calibration of the planar redundant parallel mechanism Sliding Star and calibration of the spatial fiber-driven mechanism Quadrosphere. Regarding the Sliding Star calibration, two criterion functions were used during the calibration process as terminate conditions calibrability and the mean constraint equation discrepancy. In case of the neuro-fuzzy calibration, it is advantageous to set up additional conditions that would check a maximal number of the LLMs and also set up a condition for minimal improvement of the calibrability in order to avoid overlearning and addition of unnecessary local linear models and their parameters to the calibration model. The calibration model of Quadrosphere used two multiple-input multiple-output local linear model trees for each prismatic kinematical pair of the mechanism.

https://doi.org/10.1017/S0263574715000429 Published online by Cambridge University Press

A set of equations that expresses relation between position of the working platform, mechanism frame and length of connecting fibers was used to form boundary condition of the calibration task**.** First, the simulated measurement data were used for the tuning of the calibration algorithm. This provided the option to simulate various nonlinear properties of the mechanism and properly verity the application of the calibration method on spatial fiber mechanisms. Subsequently after the mounting of the mechanism, the calibration has been applied to the mechanism and the calibrated parameters used in the control law of Quadrosphere. It can be summarized, that the main novelty and advantage of the developed calibration method is its adaptability. The complexity of the model of particular components (e.g. kinematical joints) does not need to be defined before the calibration. It is adaptively modified during the calibration process with the experimental data. The potential problem of the method lies in the increasing number of calibration parameters and consequent danger of deterioration of condition number or calibrability of the problem. Nevertheless, the chosen neuro-fuzzy models preserve the good calibrability for the increasing set of parameters. The described calibration method represents a promising approach to calibration of different types of mechanisms including the complex parallel redundantly actuated ones. It allows to obtain more precise models and parameters of the mechanisms that are necessary for their control systems in order to reach more accurate positioning during operations.

Acknowledgements

The authors appreciate the kind support by the grant GA101/11/1627 "Tilting Mechanisms Based on Fiber Parallel Kinematical Structure with Anti-backlash Control" of the Czech Science Foundation and the grant GA13-39057S "Position Feedback Based Stiffness Increase of Robots by Redundant Measurement" of the Czech Science Foundation.

References

1. P. H. Borgstrom, "Rapid computation of optimally safe tension distributions for parallel cable-driven robots," *IEEE Trans. Robot.* **25**(6), 1271–1281 (2009).
2. M. Valášek and M. Karásek, "HexaSphere with Cable Actuation," *Recent Advances in Mechatronics 2008–2009*, Springer-Verlag, Berlin (2009) pp. 239–244.
3. S. Lahouar, E. Ottaviano, S. Zeghoul, L. Romdhane and M. Ceccarelli, "Collision free path-planning for cable-driven parallel robots," *Robot. Auton. Syst. - RaS*, **57**(11), 1083–1093 (2009).
4. P. H. Borgstrom, "A cable-driven robot with self-calibration capabilities," *IEEE Trans. Robot*. **25**(5), 1005–1015 (2009).
5. M. Abderrahim, A. Khamis, S. Garrido and L. Moreno, "Acuracy and Calibration Issues of Industrial Manipulators," *Industrial Robotics: Programming, Simulation and Applications. Advanced Robotic Systems International & Pro Literatur Verlag* (2006) pp. 131–146.
6. J. Jauregui, E. Hernandez, M. Ceccarelli, C. Lopez-Cajun and A. Garcia, "Kinematic calibration of precise 6-DOF stewart platform-type positioning systems for radio telescope applications," *Frontiers Mech. Eng.* **8**(3), 252–260 (2013).
7. E. E. Hernández-Martínez, C. S. López-Cajún and J. C. Jáuregui-Correa, "Calibration of parallel manipulators and their application to machine tools," *Ing. Investigación y Tecnol.* **11**(2), 141–154 (2010).
8. B. W. Mooring, Z. S. Roth and M. R. Driels, *Fundamentals of Manipulator Calibration*, (New York: Wiley, 1991).
9. S. Y. Nof, *Handbook of Industrial Robotics*, (New York: Wiley, 1999).
10. J. M. Renders, E. Rossignol, M. Becquet and R. Hanus, "Kinematic calibration and geometrical parameter identification for robots," *IEEE Trans. Robot. Autom.* **7**(6), 721–732 (1991).
11. J. Angeles, "On the nature of the cartesian stiffness matrix," *Ing. Mec. Tecnol. Y Desarrollo*, **3**(5), 163–170 (2010).
12. D. Xuechao, Q. Yuanying, D. Qingjuan and D. Jingli, "Calibration and motion control of a cable-driven parallel manipulator based triple-level spatial positioner," *Adv. Mech. Eng.*, **2014**, Article ID 368018, 1–10 (2014).
13. Y. J. Chiu and M. H. Perng, "Self-calibration of a general hexapod manipulator with enhanced precision in 5-DOF motions," *Mech. Mach. Theory*, **39**(1), 1–23 (2004).
14. P. Miermeister, A. Pott and A. Verl, "Auto-Calibration Method for Overconstrained Cable-Driven Parallel Robots," *Proceedings of the ROBOTIK 2012; 7th German Conference on Robotics*, Munich (May 21–22, 2012) pp. 301–306.
15. T. Skopec, Z. Šika and M. Valášek, "Measurement and improved calibration of parallel machine sliding star," *Bull. Appl. Mech.* **6**(23), 52–56 (2010).

https://doi.org/10.1017/S0263574715000429 Published online by Cambridge University Press

16. O. Nelles, Nonlinear System Identification with Local Linear Neuro-Fuzzy Models *PhD Thesis* (Darmstadt: Technische Universitat Darmstadt, 1998).
17. O. Nelles, *Nonlinear System Identification: From Classical Approaches to Neural Networks and Fuzzy Models* (Berlin: Springer, 2001).
18. M. Valášek, Z. Šika, J. Zavřel, T. Skopec and P. Steinbauer, "Control Rapid Prototyping of Redundantly Acutated Parallel Kinematical Machine," *Technical Computing Prague* (Prague: Humusoft, 2006), pp. 1–10.
19. Z. Šika, V. Hamrle, M. Valášek and P. Beneš, "Calibrability as additional design criterion of parallel kinematic machines," *Mech. Mach. Theory*, **50**, 48–63 (2012).
20. P. Svatoš , Z Šika, M. Valášek, V. Bauma and P. Polach, "Optimization of anti-backlash fibre driven parallel kinematical structures," *Bull. Appl. Mech.* **8**(31), 40–44 (2012).
21. M. Valášek, and M. Karásek, "Kinematical Analysis of HexaSphere," *Proceedings of Engineering Mechanics 2009*, Svratka, Czech Republic (May 11–14, 2009) pp. 1371–1378.
22. M. Valášek, J. Zicha, J. Karásek and R. Hudec, "Hexasphere—Redundantly Actuated Parallel Spherical Mechanism as a New Concept of Agile Telescope. *Advances in Astronomy*, **2010**, Article ID 348286, 1–6 (2010).
23. L. Sciavicco and B. Siciliano, *Modeling and Control of Robot Manipulators* (New York: McGraw-Hill, 1996).
24. V. Stejskal and M. Valášek, *Kinematics and Dynamics of Machinery* (New York: Marcel Dekker, Inc., 1996).
25. R. Kurtz and V. Hayward, "Multiple-goal kinematic optimization of a parallel spherical mechanisms with actuator redundancy," *IEEE Trans. Robot. Autom.* **8**(5), 644–651 (1992).

https://doi.org/10.1017/S0263574715000429 Published online by Cambridge University Press